Appendix A

This section summarizes the Rotational Isomeric State (RIS) tables and the charges on the five polymer samples (PET, PP, PCTFE, PVDC and PVOH) selected for the present solubility study. The RIS table contains information on the conditional probability of key dihedral angles in the polymer chain determined by separately minimizing the energy of the representative torsions, with coupling where applicable. The charges on the polymers are calculated from electrostatic potential fits (ESP) to Hartree Fock (6-31G** basis set) quantum charges using the Jaguar program (Schrödinger LLC). The atomic charges for the monomer structures are calculated first after replacing the head and tail atoms (hydrogens) by methyl groups (CH_3) to avoid terminal edge effects on the charges. A macro is then used to assign the Jaguar calculated quantum charges back to the monomer after first replacing the terminal methyl groups with hydrogen atoms. The residual charge is redistributed over the entire monomer, except for the terminal hydrogen atoms that remained uncharged. The terminal hydrogens are used as dummy atoms for the monomer as they are deleted when a polymer chain is generated. The monomer configuration with ESP charges is used to build a trimer and to determine the main representative torsions of the PET polymer.

A1. Polyethylene terephtalate (PET)

The structure of the PET monomer (Fig. 2) is loaded from the Cerius[2] [**Error! Bookmark not defined.**] database. By including only main backbone atoms (side chains are easily realigned by dynamics), three representative torsions are selected. The torsions are

denoted as t_1 (all $C\_3-O\_R-C\_3-C\_R$ type), t_2 (all $C\_3-O\_R-C\_3-C\_3$ type) and t_3 (all $O\_R-C\_3-C\_3-O\_R$ type), respectively. To optimize the polymer geometry by calculating the torsional potentials and the Rotation Isomeric Structure (RIS) table, torsion t_1 is minimized first. Torsions t_2 and t_3 are then minimized after coupling with t_1, and t_2, respectively.

For torsion t_1, the energy variation as a function of the total number of conformations of the trimer (Fig. A1.1) indicates the presence of three local minima of the energy, each corresponding to a representative state of the polymer. Table A1.1 summarizes the angle values and their tolerances that correspond to these local minima in the energy.

For the analysis of the coupled t_1-t_2 and t_2-t_3 torsions, density contours are analyzed (Fig. A1.2). The dark blue regions correspond to a low probability (low energy) of correlation angles. The degree of correlation increases with color brightening. Fig. A1.2 indicates the existence of two local minima for the t_2 torsion (Table A1.2). The presence of the double bonded oxygen in the close vicinity of the resonant carbon makes it difficult for the structure to bend or flex. It seems that the optimal conformation occurs when the double bonded oxygen and the carbon-carbon resonant bond remain in the same plane.

Compared to the t_1-t_2 coupling, the t_2-t_3 coupled torsion has a higher number of states (Table A1.3) most probably because none of the two component torsions contains a resonant carbon that would restrain the structural freedom.

The RIS table is built by compiling Tables A1.1-A1.3 and thus contains all the key information characterizing the representative states of equilibrium (or local equilibrium) of the polymer. For all three investigated cases (t_1, t_1-t_2, t_2-t_3) the given tolerances for the angles actually represent the range of variation that corresponds to a change in energy of 1%. The RIS table is

used as input for the CED procedure (section 2 and [**Error! Bookmark not defined.**]) in which amorphous samples of a three dimensional periodic unit cell of the polymer are constructed. The charges for the PET monomer and trimer are summarized in (Table A1.4).

A2. Polyvinylidene chloride (PVDC) and polyvinyl alcohol (PVOH)

Both polymers, PVDC and PVOH, have a representative torsion, t_1, defined by the backbone carbon atoms (C-C-C-C). The torsion energy distribution is determined for the dimer as it contains the minimum number of monomers for which this torsion is defined. The angles and energetic minima for PVDC and PVOH are summarized in Table A2.1. The atomic charges for PVDC and PVOH are shown in Fig. A2.1.

A3. Polypropylene (PP)

The torsional potential for PP (Fig. A3.1) is determined via a grid scan (from –180 to 175 degrees in steps of 5 degrees) on the middle torsion of the polypropylene pentamer and indicates a relatively rotatable bond. The energy difference between the lowest and highest energy conformers is about 10 kcal/mol. From this potential plot, an RIS table (Table A3.1) is created and used to prepare the CED samples (syndiotactic PP, 20-mer).

The atomic charges for the PP system are calculated using quantum mechanics (Table A3.2), then averaged out to create a neutral monomer that is repeated to generate the polypropylene polymer.

A4. Polychlorotrifluoroethylene (PCTFE)

PCTFE has a chiral center at the carbon bonded to both a chlorine and a fluorine atom. Because of this chiral center, tacticity had to be taken into consideration. Syndiotactic polymers are generated. The PCTFE polymer is defined by two torsional angles. The most central torsion is used for both dihedrals. A simple, uncoupled RIS energy table is generated for the first torsion (Table A4. 1). To describe the coupling between the two torsional angles, a coupled RIS table is then generated (Table A4. 2). A grid scan is run through the 5,184 conformers generated from all the combinations taken for the two torsion angles (scanning angles from –180 to 175 degrees in 5 degree intervals). The dreidii-exp6-direct.par force field is used for this conformer search. The corresponding Ramachandran plot is shown in Fig. A4.1. The atomic charges of the PCTFE monomer and trimer are summarized in Table A4.3.

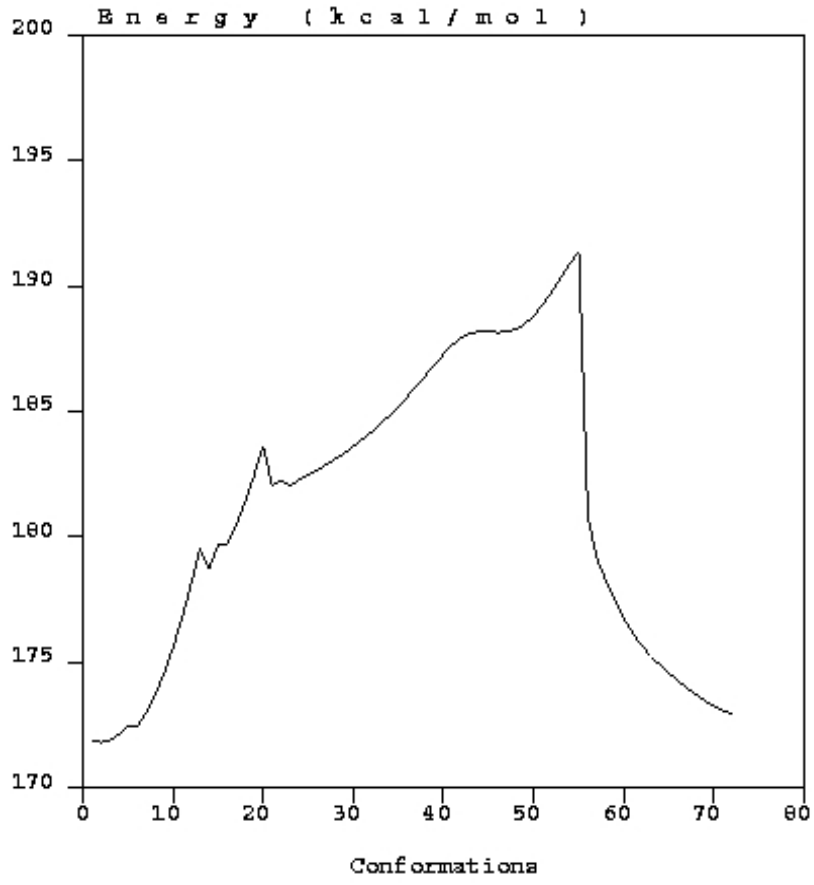

Figure A1.1. Energy (kcal/mol) as function of the total number of conformation for torsion t_1 (all atoms with C_3-O_R-C_3-C_R type) of PET.

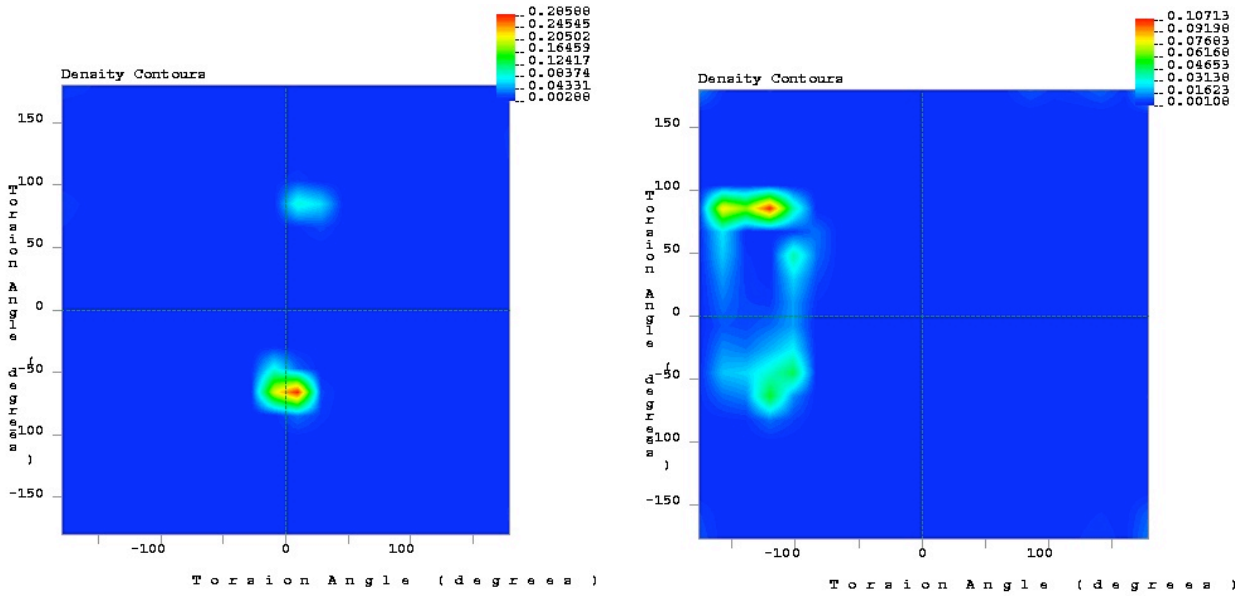

Figure A1.2. Density contours for coupled torsions t1-t2 and t2-t3 in PET. Dark blue regions correspond to low correlated torsions (low energies) while the correlation degree increases the brighter the color.

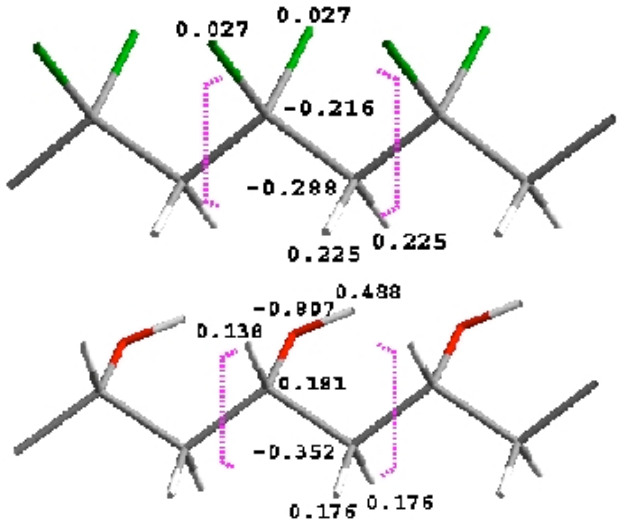

Figure A2.1. Atomic charges on PVDC (top) and PVOH (bottom) from quantum mechanics.

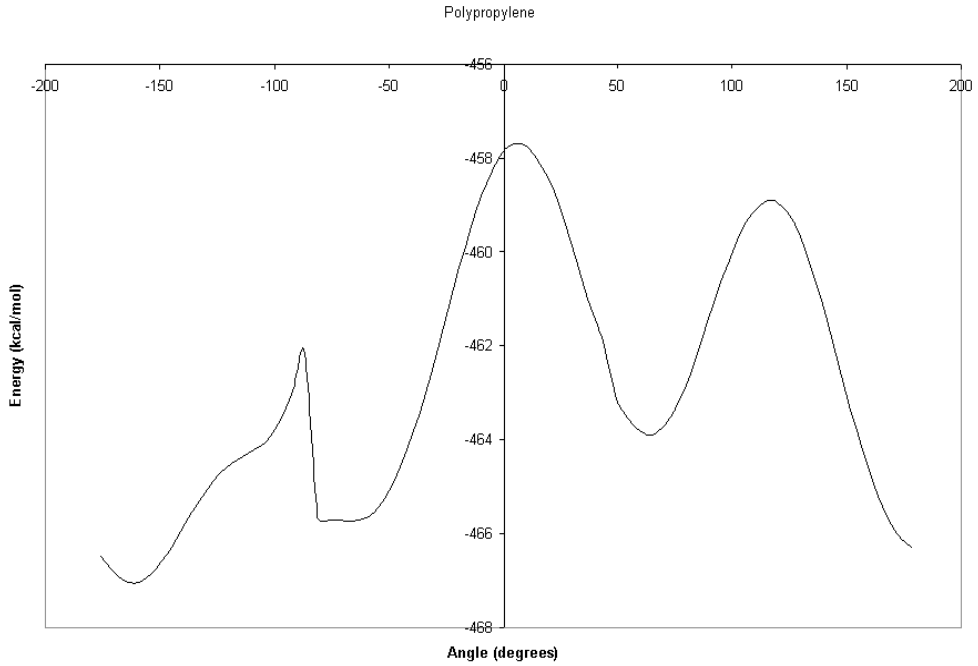

Figure A3.1. Torsional potential for the main torsion of PP.

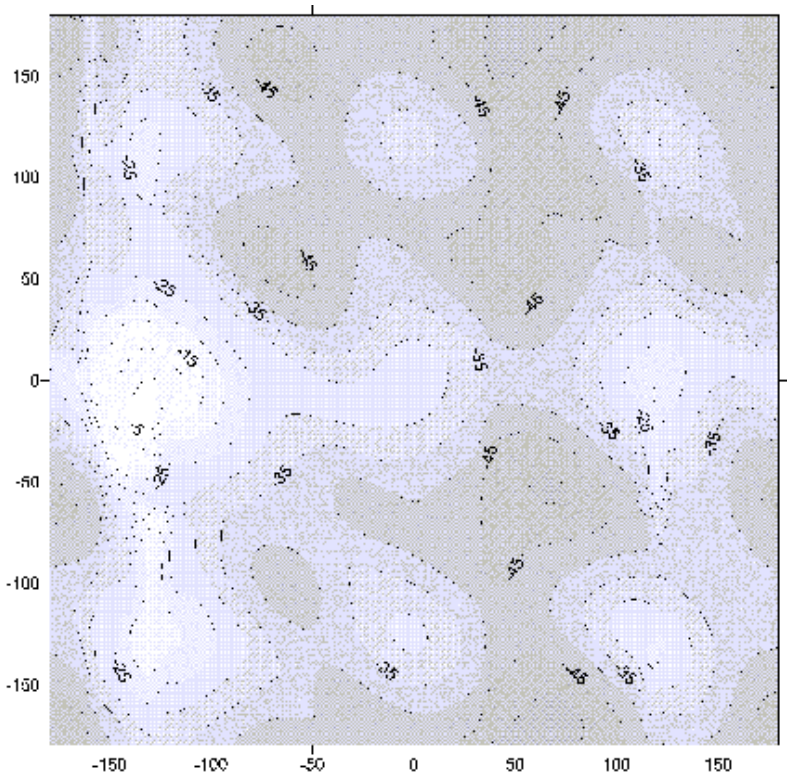

Figure A4.1. Torsional potential for the main torsion of PCTFE.

Table A1.1. Angles and energies characterizing the three representative t_1 states of PET.

Angle deg	Tolerance deg	Energy kcal/mol
45.0	10.0	188.2
185.0	10.0	171.8
290.0	10.0	182.1

Table A1.2. Representative states for coupled t_1-t_2 torsions for PET.

$T_1 \backslash T_2$ deg	Δt_2 deg	29.0	14.3
74.9	25.0	161.0	155.0
275.0	30.0	155.0	151.6

Table A1.3. Representative states for coupled t_2-t_3 torsions for PET.

T_3/T_2 deg	Δt_3 deg	207.0	248.0	264.0
34.0	20.0	200.0	200.0	150.3
66.0	10.0	149.5	149.3	200.0
294.0	10.0	200.0	150.6	200.0
309.0	5.0	150.8	200.0	200.0

Table A1.4. Atomic charges of the PET monomer.

Atom	Charge in monomer	Charge in trimer (ESP)
C1	0.65606	0.66205
C2	-0.12530	-0.11931
H3	0.13972	0.14571
C4	-0.15101	-0.14502
H5	0.13896	0.14495
C6	-0.08504	-0.07905
C7	-0.10243	-0.09644
H8	0.14725	0.15324
C9	-0.11571	-0.10972
H10	0.13693	0.14292
C11	-0.09128	-0.08529
O12	-0.55509	-0.54909
C13	0.77351	0.77950
O14	-0.46129	-0.45529
O16	-0.53615	-0.53016
C17	0.08063	0.08662
H18	0.09454	0.10053
H19	0.07788	0.08387
C20	0.21222	0.21821
H21	0.02388	0.02987
H22	0.04991	0.05590
O23	-0.44006	-0.43407

Table A2.1. Angles and energies characterizing the three representative t_1 states of PVDC.

Polymer	Angle deg	Tolerance deg	Energy kcal/mol
PVDC	50.0	10.0	16.101
	85.0	10.0	18.918
	310.0	10.0	16.117
PVOH	50.0	20.0	1.054
	175.0	10.0	0.000
	260.0	12.0	4.088
	290.0	10.0	4.720

Table A3.1. Angles and energies characterizing the three representative t_1 states of PP.

Angle deg	Toleranc deg	Energy kcal/mol
45.0	10.0	1.000
240.0	2.0	3.000
320.0	4.0	0.000

Table A3.2. Atomic charges of the PP monomer.

Atom	Charge in monomer	Charge in trimer
C (tail)	-0.5576	-0.55904
H	0.1304	0.12900
H	0.1035	0.10204
C (head)	0.5393	0.53785
H	-0.0549	-0.05636
C (methyl group)	-0.4961	-0.49754
H	0.1219	0.12044
H	0.1033	0.10192
H	0.1103	0.10890

Table A4.1. Angles and energies characterizing the three representative t_1 states of PCTFE.

Angle deg	Tolerance deg	Energy kcal/mol
0.0	5.0	4.000
120.0	5.0	4.000
230.0	10.0	0.000

Table A4.2. Representative states for coupled t_1-t_2 torsions of PCTFE.

$T_1 \backslash T_2$ deg	Δt_2 deg	0.0	120.0	230.0
0.0	15.0	4.000	4.000	0.000
130.0	3.0	4.500	4.500	0.500
232.0	5.0	4.750	4.750	0.750

Table A4.3. Atomic charges for the PCTFE monomer.

Atom	Charge in Monomer	Charge in Trimer
C (chiral center; attached to head)	-0.1887	-0.18360
Cl	0.0776	0.08271
F (attached to chiral center)	-0.0215	-0.01644
C (attached to tail)	0.4128	0.41789
F (labeled F13)	-0.1413	-0.13623
F (labeled F14)	-0.1390	-0.13392

Appendix B

It is critical for the accuracy of the calculated solubility data that the properties of the polymer matrix are correctly simulated. From the simulated temperature dependence of the polymer's average unit cell volume and density, the melting temperature is estimated. Additionally, the temperature variation of the bulk modulus, the compressibility and the thermal expansion coefficient are calculated (section B1). This information is then compared with experimental data.

The amount of fluctuations during the dynamics (NPT) of the polymer is determined by the value selected for the mass cell pre-factor (MCPF). Section B2 discusses the effect of various values of MCPF on the simulated polymer dynamics also in relation with the time variation observed for Henry's constant.

B1. Compressibility and thermal expansion coefficients

The MD average of the total, occupiable and available volume shows a linear increase with temperature (Fig. B1.1). However, both graphs exhibit a discontinuity between 450 K and 550 K approximately corresponding to the melting regime of PP. Additionally, Fig. B1.2 shows the temperature variation of the density of syndiotactic PP for which experimental densities are available below melting, between 300 K and 473 K [**Error! Bookmark not defined.**]. The agreement between calculated and experimental densities is better for temperatures above the melting point.

From the temperature dependence of the average volume/density, a value of 577 K is predicted from our calculations as the melting temperature of PP. This value is determined from the equality of the linear fits of the data points below and above 500 K (Fig. B1.1).

Three factors, the isothermal compressibility, the bulk modulus and the thermal expansion coefficient, can be calculated from MD simulations as control factors for the accuracy with which the simulation reproduce the experimental data.

From the volume fluctuations of the unit cell during the polymer's dynamics, the *isothermal compressibility*, α (GPa^{-1}), is calculated according to:

$$\alpha = \frac{\langle V^2 \rangle - \langle V \rangle^2}{\langle V \rangle k_B T} \qquad \textbf{(11)}$$

with <> the notation for ensemble averaging, V the total unit cell volume, k_B Boltzmann's constant ($=1.38 \cdot 10^{-23}$ JK^{-1}) and T (K) the absolute temperature. By definition, *the bulk modulus*, β (GPa), is calculated as the inverse of the isothermal compressibility, α. At each temperature, the *thermal expansion coefficient*, α_T (K^{-1}), is calculated from the linear fit of the volume versus temperature as the slope of V (T) divided by the average MD volume corresponding to temperature T.

Experimental compressibility data is available for melted PP. Table B1.1 shows that for temperatures between 450K and 550K the isothermal compressibility values calculated in the present study follow the same trend as the experimental data although underestimated by about 15-30%.

Experimental values for the thermal expansion coefficient are available for a broad range of temperatures whereas compressibility data is available only for melted PP. The variation of the thermal expansion coefficient with temperature is shown in Fig. B1.4. The agreement is

good for temperatures above 450K (above T_{melt}, 10% high), but the predicted values (Table B1.2) are high by a factor of 8 near the glass temperature (280K).

Actually it is more accurate to describe the melting of a polymer as a process that takes place over a range of temperatures, depending on many factors (i.e., molecular weight, chain stiffness, degree of branching, etc.). The data points in Fig. B1.1 - Fig. B1.4 indicate that the PP melting process starts somewhere between 400 K and 450 K and is completed around 550 K.

Depending on the extrapolation technique used to calculate melting temperatures from experimental data a range between 415K and 477 K is determined for syndiotactic PP for the equilibrium melting temperature [29]. The 477 K value corresponds to 100% syndiotactic PP. For comparison, for isotactic PP the melting temperature ranges from 398 K to 439 K.

The values predicted in the present study are in good agreement with the experimental ranges considering that our modeled polymer has a lower molecular weight where it is observed that increasing the mass or chain length results in raising the melting temperature.

B2. Mass cell pre-factor coefficient

In the Rahman-Parrinello approach (the barostat used in the NPT calculations to preserve constant pressure in the system) a user-defined mass-like parameter corresponding to the volume dynamical variable is used to calculate the kinetic energy of the cell. This represents actually the piston mass and is considered in the dynamics as a mass cell pre-factor (MCPF) controlling the heat flow rate. A value of 1 for MCPF is used so far in our calculations. Generally this value should be chosen such that the fluctuations in the volume are much slower

than in the temperature. In addition the volume properties should be calculated over a large number (~20) of these long-term fluctuations.

To verify the influence of the MCPF on the dynamics and the calculated k_H values, additional 100 ps of NPT dynamics at 300K are run with values of the mass cell pre-factor of 5 and 10, respectively. Fig. B2.1 shows the time variation during dynamics of the total unit cell volume for the three values of the MCPF. With increasing piston mass (larger MCPF values), the volume space is less explored and the volume fluctuations decrease in amplitude and periodicity. Too small values selected for MCPF result in fast motion of the cell vectors but could induce artificial periodic motions of the cell and may not allow enough time for equilibration. Larger values of MCPF mean a heavy, slow fluctuating cell (for infinite value of MCPF constant-volume dynamics should be obtained) thus, requiring longer dynamics runs. Here it appears that the 100 ps of sampling is sufficient for MCPF=1 and 5, but perhaps not for MCPF=10. Consistent with the volume fluctuations, the compressibility is also not well represented for large values of the MCPF (Fig. B2.2).

The time variation of k_H calculated using the Henry's constant ensemble from the NPT-MD simulations at 300K for each of the three values of MCPF (1, 5 and 10, respectively) is shown in Fig. B2.3. The limits for a 95% confidence interval of k_H and the average total unit cell volumes are summarized in Table B2.1. Both, Fig. B2.3 and Table B2.1 indicate that it would be beneficial for the accuracy of the calculated k_H values to allow a slower exploration of the volume (MCPF=10) as the time fluctuation and the limits of the confidence interval calculated for k_H for MCPF=10 are smaller than for MCPF=5 and MCPF=1. However, by exploring less the volume space, fewer polymer configurations are also sampled and representative contributions may be lost. Using a larger value for MCPF would mainly result in increasing the

simulation time. This analysis proves that the choice of a MCPF value of 1 is optimal from the point of view of exploration of the volume domain and the required simulation time.

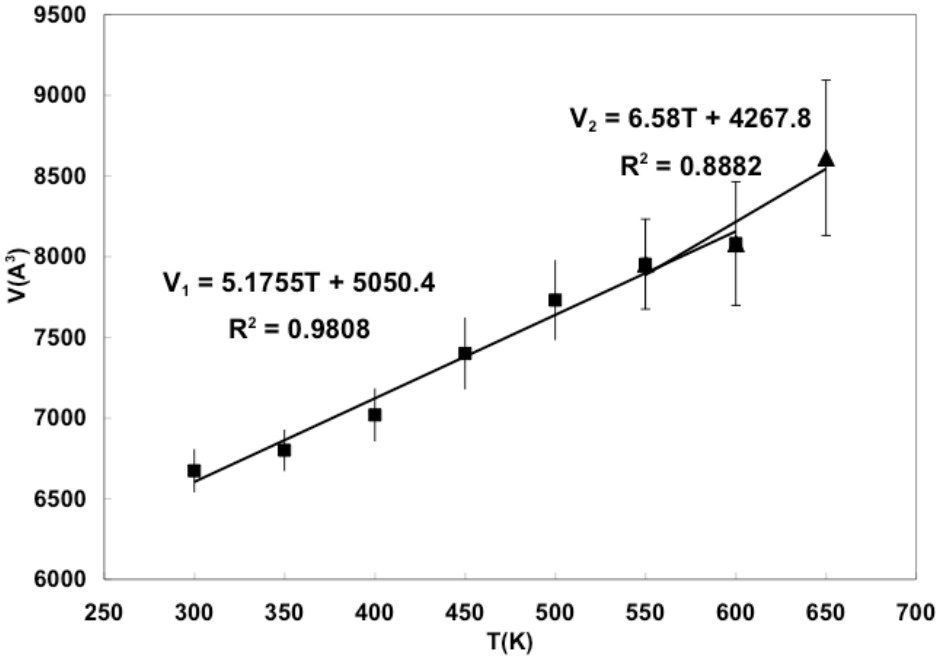

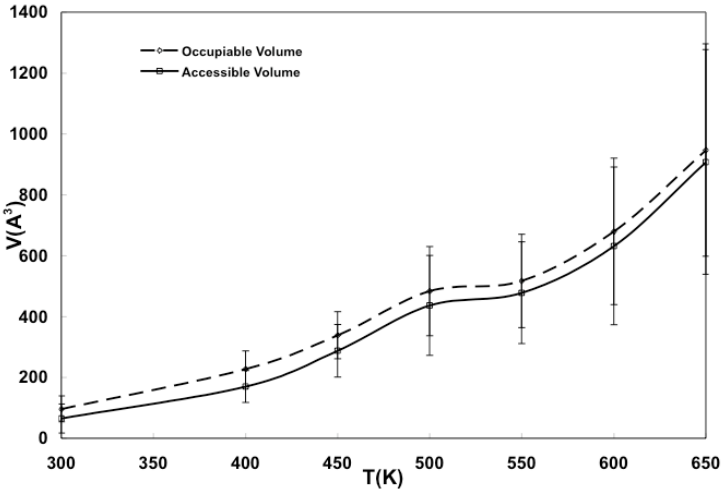

Figure B1.1. Temperature dependence of the MD-averaged unit cell total volume of PP. The inset represents the temperature dependence of the occupiable and accessible volumes.

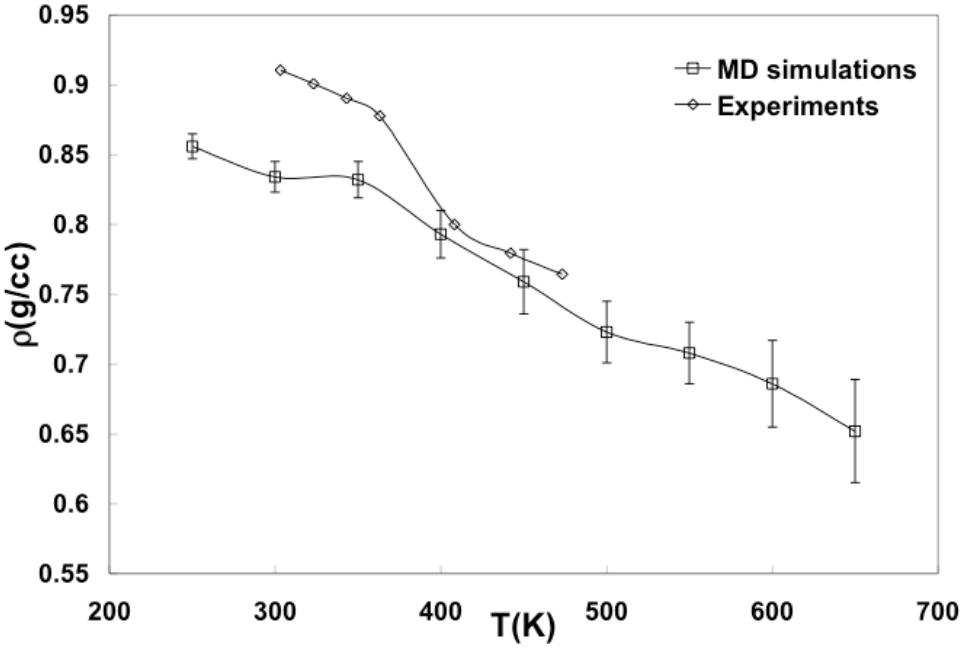

Figure B1.2. Temperature variation of PP density from MD simulations (squares). For comparison, experimental data (diamonds) are also shown [**Error! Bookmark not defined.**].

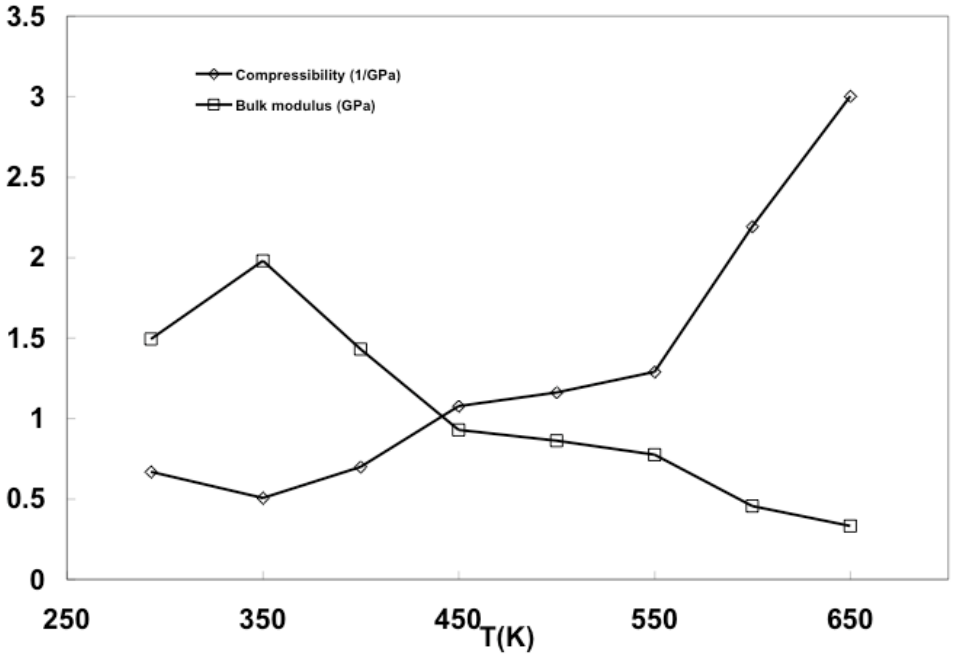

Figure B1.3. Temperature variation of compressibility, α, and bulk modulus, β, for PP.

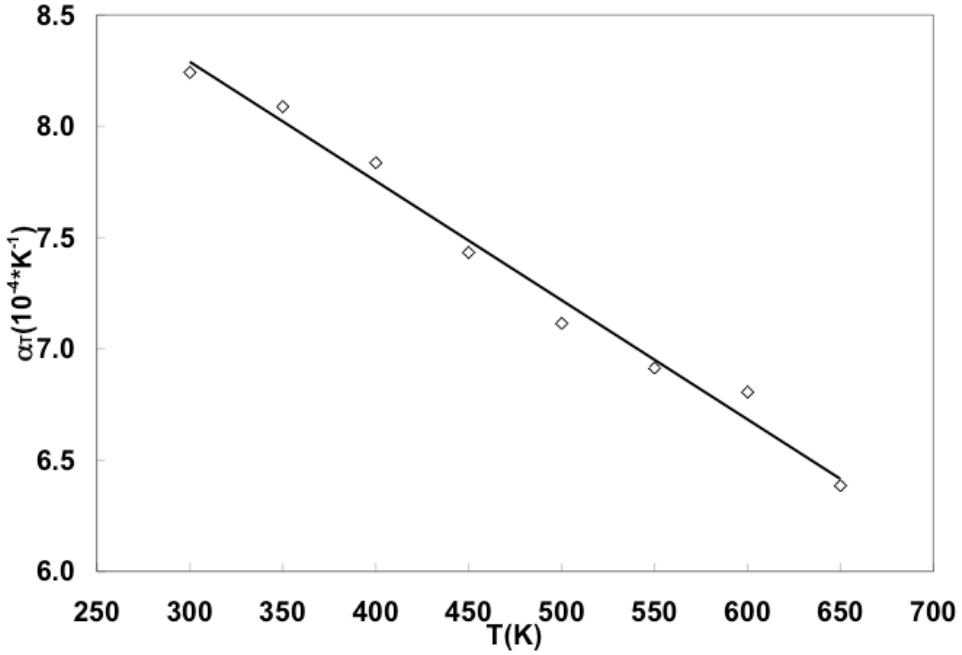

Figure B1.4. Temperature variation of the thermal expansion coefficient, α_T, of PP.

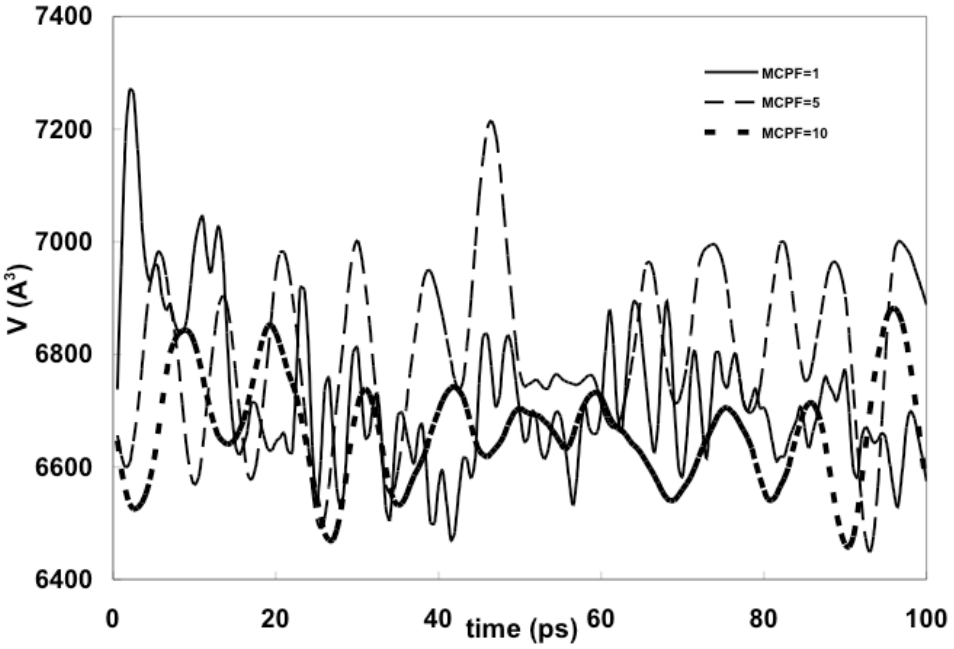

Figure B2.1. Time variation of unit cell volume for PP at 300K as function of the MCPF used in dynamics (150 ps NPT).

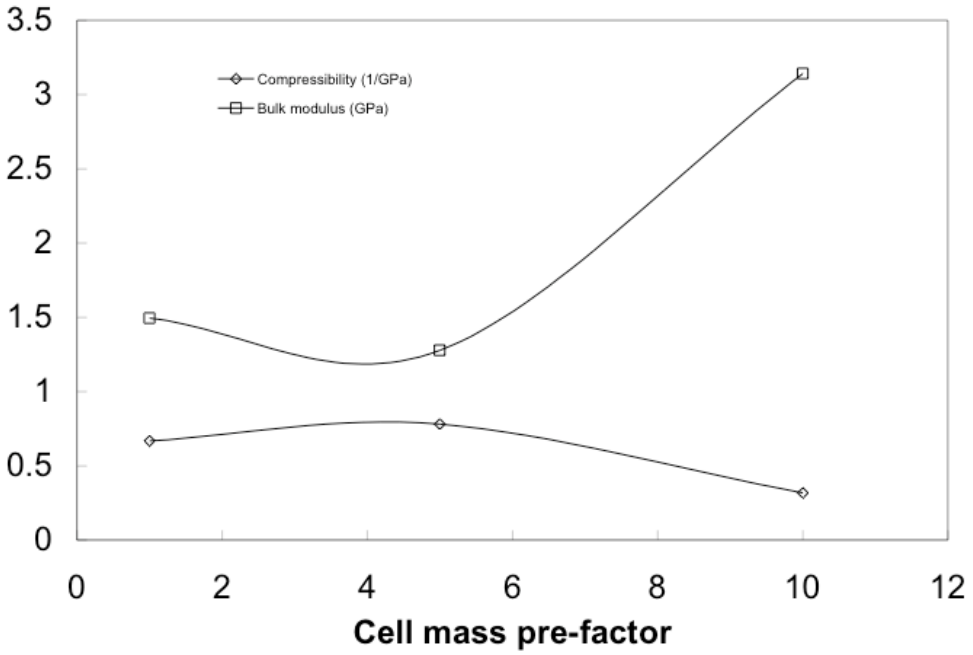

Figure B2.2. Dependence of compressibility and bulk modulus on the value (1, 5 and 10) of the cell mass pre-factor (MCPF) set in the NPT dynamics calculation at 300K for PP.

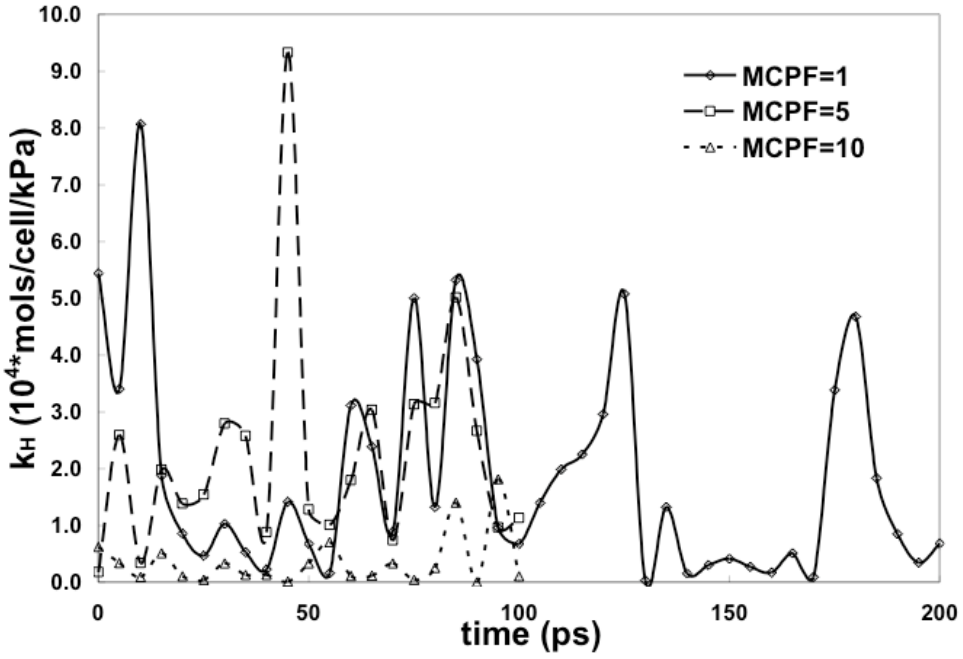

Figure B2.3. Time variation of Henry's constant, k_H, calculated from NPT dynamics for PP at 300K using three values for the mass cell pre-factor, MCPF, in the Rahman-Parrinello barostat.

Table B1.1 Coefficient of isothermal compressibility, $\alpha(GPa^{-1})$, for PP.

T (K)	experiment [**Error! Bookmark not defined.**]	present study
453	1.27	1.08(450K)
493	1.5	1.16 (500K)
533	1.78	1.29 (550K)

Table B1.2 Coefficient of linear thermal expansion and of thermal expansion (melt), α_T (K^{-1}) for PP.

T(K)	experiment [**Error! Bookmark not defined.**]	present study
243-273	6.5e-5	
273-303	1.1e-4	8.24e-4
303-330	1.4e-4	8.09e-4
448-573	6.6e-4	7.43e-4 to 6.81e-4
453-503	6.7e-4	

Table B2.1. Confidence intervals of k_H calculated for N_2 in PP at 300K corresponding to three values of the mass cell pre-factor (MCPF) in the Rahman-Parrinello barostat. The averages of the total unit cell volume, V, over the MD simulation times, t, are also indicated.

MCPF	t ps	V Å^3	k_H cc^3/kg/MPa
1	200	6672±135	(838< k_H ≤1590)
5	100	6807±149	(879< k_H ≤2010)
10	100	6660±94	(99< k_H ≤368)